ISSN 1990-7931, Russian Journal of Physical Chemistry B, 2019, Vol. 13, No. 5, pp. 763–768. © Pleiades Publishing, Ltd., 2019.
Russian Text © The Author(s), 2019, published in Khimicheskaya Fizika, 2019, Vol. 38, No. 10, pp. 41–47.

ELECTRICAL AND MAGNETIC PROPERTIES OF MATERIALS

Structure and Sensing Properties of Nanostructured SnO_2–In_2O_3 Composites Synthesized by the Impregnation Method

G. N. Gerasimov[a, b], V. F. Gromov[a, b], M. I. Ikim[a, *], E. Yu. Spiridonova[a, b], M. M. Grekhov[c], and L. I. Trakhtenberg[a, b]

[a] *Semenov Institute of Chemical Physics, Russian Academy of Sciences, Moscow, 119991 Russia*
[b] *Karpov Institute of Physics and Chemistry, Moscow, 105064 Russia*
[c] *National Research Nuclear University MEPhI, Moscow, 115409 Russia*
**e-mail: ikim1104@rambler.ru*

Received December 21, 2018; revised December 21, 2018; accepted January 21, 2019

Abstract—The structure and sensing properties of SnO_2–In_2O_3 composites synthesized by the impregnation method are studied. These composites consist of In_2O_3 nanocrystals comprising SnO_2 nanoclusters with a size of 5–7 nm on their surface. Using energy-dispersive X-ray spectroscopy, it is found that the SnO_2 nanoclusters contain indium ions, which provide an increase in the number of catalytically active oxygen vacancies in them. The maximum efficiency of the synthesized composites for hydrogen detection in air is achieved at a SnO_2 content in the composite of about 40 wt %. In this case, the high sensor sensitivity of the composite is attributed to the catalytic activity of SnO_2 clusters containing indium ions and the high specific surface area of SnO_2 aggregates, which provide the conductivity of the composite.

Keywords: nanocomposite, impregnation method, cluster, sensor response, hydrogen
DOI: 10.1134/S1990793119050154

INTRODUCTION

The ever-growing challenges associated with environmental pollution and safety show the necessity of real-time environmental monitoring. To this end, nanocrystalline semiconductor metal oxides, whose electrical conductivity varies depending on the composition of the surrounding gas atmosphere, are currently used as sensors to detect reducing gases, such as hydrogen, hydrocarbons, and carbon monoxide. The sensor effect is attributed to a change in the electrical conductivity of the sensor caused by the chemical (sensory) reaction of the gas with anionic oxygen centers on the surface of the sensor nanocrystals [1–3]. This reaction, which is accompanied by the release of trapped electrons and their transition into the conduction band of metal oxide, leads to an increase in the electrical conductivity of the sensor.

The sensing properties of a nanostructured metal oxide system are determined by its morphology, the electronic structure of the particles, and the interaction between them [4, 5]. In this context, new possible designs of efficient fast-response sensors are enabled by the use of composite systems consisting of metal oxides with different electronic and catalytic properties. Depending on the nature and content of components in this composite, the sensitivity and selectivity of the composite change as it detects different compounds (see, e.g., [6–8]).

Sensor effects in binary metal oxide systems are founded in the specific contacts between dissimilar metal oxide particles and the incorporation of ions of one metal oxide into the crystal lattice of the other, which can occur during the formation of the composite. Of particular importance for the sensing properties of a nanostructured metal oxide semiconductor composite is the morphology of the composite and in particular, the size of nanoparticles involved in the sensory process. A decrease in the size of the nanoparticle leads to an increase in the specific surface area of the sensitive layer of the sensor, resulting in an increase in the concentration of oxygen and analyte gas molecules chemisorbed in this layer, which leads to an enhancement of the sensor effect [9, 10]. It is particularly important that the characteristic structural flexibility of nanocrystalline metal oxide grains that are smaller than 10 nm under the action of stresses generated by the incorporation of foreign ions into their lattice opens up possibilities of the directed modification of nanoparticles to improve the sensitivity and selectivity of a sensor. In particular, it is shown that, in the case of doping of SnO_2 with indium ions, their dissolution in the SnO_2 lattice is observed only for SnO_2 nanoparticles with a size of 5–10 nm [11].

The size of a nanoparticle in a nanostructured composite depends on the method of formation of the composite. It has been found that the impregnation of

metal oxide nanocrystals with a metal salt solution and the subsequent heat treatment of the impregnated sample under certain conditions lead to the formation of another oxide with a size of up to 10 nm on the surface of matrix nanocrystals of metal oxide nanoclusters [12–15]. In this study, nanocomposites consisting of In_2O_3 nanocrystals with a size of 30–40 nm, which contain SnO_2 nanoclusters with a size of 5–8 nm on their surface, are synthesized by the impregnation method. The structure, electrical conductivity, and sensing characteristics of the resulting nanocomposites for hydrogen detection are studied. It is shown that high sensor sensitivity is achieved in the case of a certain composition of the nanocomposite provided by its specific structure.

EXPERIMENTAL

The SnO_2–In_2O_3 composites were synthesized by impregnating In_2O_3 nanocrystals with an aqueous solution of $SnCl_4$ and subsequently subjecting the impregnated samples to a heat treatment. Commercial In_2O_3 nanopowder samples (AnalaR grade, 99.5%, BDH/Merck Ltd., Lutterworth, Leicestershire, UK) were used. To prepare the samples, a suspension of In_2O_3 nanocrystals in an aqueous solution of $SnCl_4$ was stirred for 24 h and then held for 24 h to provide a uniform penetration of the solution into all of the pores of the powder. The $SnCl_4$ concentration in the solution was 0.014 mol/L. After that, water was evaporated in air at 70°C; the resulting impregnated powder was held at 100°C for 5 h and then heated in air at 500°C for 5 h. This heat treatment led to the hydrolysis of tin chloride and the subsequent formation of SnO_2. The tin oxide content in the synthesized impregnated composite was calculated according to the amount of the salt added per gram of the In_2O_3 powder to the initial suspension.

To determine the conductivity and sensing properties of the synthesized materials, they were mixed with distilled and deionized water. The resulting paste was deposited on polycor plates and annealed at 550°C until a constant resistance of the resulting film was achieved.

The structure of the composites was determined by X-ray diffraction (XRD), transmission electron microscopy (TEM), and energy-dispersive X-ray (EDX) spectroscopy. The XRD spectra were recorded using a Rigaku Ultima IV X-ray diffractometer (CuK_α radiation, $\lambda = 0.154056$ nm) that was equipped with a narrow slit analyzer providing an increase in the resolution of XRD patterns and a graphite monochromator providing the detection of weak peaks in XRD patterns.

Average nanoparticle size (D) was determined from XRD spectra in accordance with the Debye–Scherrer formula: $D = 0.9\lambda/(\beta\cos\theta)$, where λ is the X-ray wavelength, β is the peak half-width, and θ is the diffraction angle corresponding to this peak. The relative position and contacts of particles in the composites were determined by TEM on a JEM-2100 instrument (Jeol, Japan). The EDX spectra, which characterize, in particular, the distribution of metal ions between the composite components, were recorded on a JOEL JSM-5610 instrument equipped with an Oxford Instruments X-MaxN 100TLE EDX microanalysis system.

The sensory activity of the composites in hydrogen detection was measured in a temperature range of 300–450°C. The temperature maintenance accuracy was ±1°C. Pure air or air containing 1100 ppm of hydrogen was pumped through a 1 cm^3 measuring chamber with the sensor placed into it at a rate of 200 cm^3/min. Sensor effect S was defined as $S = (R_0/R_g)$, where R_0 and R_g are the resistance of the sensor film in pure air and in air containing the analyte gas, respectively.

RESULTS AND DISCUSSION

The initial In_2O_3 nanocrystals have a cubic structure with a lattice parameter of 1.012 nm. The XRD analysis data showed that, in the synthesized composites, this structure of In_2O_3 crystals is preserved, while SnO_2 nanoclusters formed during impregnation have a tetragonal structure characteristic of SnO_2 crystals. The XRD data are shown in Table 1 for the (110) and (400) peaks in the tetragonal lattice of SnO_2 and in the cubic lattice of In_2O_3, respectively. These peaks were selected because they do not overlap other peaks in the spectrum of the composite even partially. The designations in Table 1 are given in accordance with the Debye–Scherrer formula. The average size D of the initial In_2O_3 nanocrystals, which was determined from the XRD data in accordance with the Debye–Scherrer formula, is 35 nm; it changes little during the formation of SnO_2–In_2O_3 composites by the impregnation of the crystals (see Table 1).

At SnO_2 concentrations of up to 10 wt %, only In_2O_3 crystals are detected in the composite. It is known that the dissolution of small amounts of SnO_2 in In_2O_3 crystals hardly changes the crystal structure [16]. The increase in the conductivity of the composite compared with the conductivity of pure In_2O_3 (Fig. 1) confirms the formation of SnO_2 solid solutions in In_2O_3 crystals. This effect is also observed in composites synthesized by codeposition of SnO_2 and In_2O_3 from a solution of tin and indium salts [17]. The effect is attributed to the fact that an increase in the localized positive charge caused by the replacement of In^{3+} in the In_2O_3 lattice by Sn^{4+} ions is compensated for by the formation of negatively charged oxygen vacancies containing electrons weakly bound to the lattice. The transition of these electrons into the conduction band of In_2O_3 leads to an increase in the conductivity of the composite at low SnO_2 concentrations, when the cur-

Table 1. X-ray diffraction data for SnO_2 and In_2O_3 crystals

SnO_2 content, %	SnO_2, tetragonal lattice, peak (110)			In_2O_3, cubic lattice, peak (400)		
	2θ, deg	β, deg	nanoparticle size, nm	2θ, deg	β, deg	nanoparticle size, nm
0	–	–	–	35.46	0.265	35
40	26.55	1.75	5	35.49	0.251	37
100	26.59	0.181	49	–	–	–

rent paths in the composite are formed by In_2O_3 crystals. It is characteristic that the In_2O_3 particles observed under a transmission microscope (Fig. 2a) are apparently aggregates of crystals recorded by XRD.

According to [18], the solubility limit of SnO_2 in In_2O_3 is 10–15 wt %, which corresponds to 5–7 at % Sn. With an increase in the SnO_2 concentration above this limit, SnO_2 nanoclusters are formed in the composite; according to XRD, the average size of these nanoclusters is about 5 nm (see Table 1).

As the SnO_2 nanoclusters accumulate, low-resistance current paths consisting of In_2O_3 nanocrystals are broken by inclusions of SnO_2 nanoclusters, whose resistance is three orders of magnitude greater than those of the In_2O_3 nanocrystals. Simultaneously, the formation and multiplication of current paths through aggregates of SnO_2 nanoclusters are observed. All these factors lead to an increase in the resistance of the composite (Fig. 1). Owing to the small size of the SnO_2 nanoclusters and, accordingly, the large width of their peaks in the XRD spectra, the resulting nanoclusters are clearly detected only at a total SnO_2 concentration of about 40 wt %. In this case, assuming that approximately 10 wt % SnO_2 is dissolved in In_2O_3, the concentration of SnO_2 nanoclusters can be estimated at 30 wt %. In the synthesized nanostructured SnO_2–In_2O_3 composites, the D_{In}/D_{Sn} ratio is ~7. Calculations based on the percolation theory [19] show that, at this D_{In}/D_{Sn} ratio, all current paths through In_2O_3 crystals are completely interrupted by SnO_2 nanoclusters at their concentration in the composite of about 30%. Thus, the final percolation transition to conduction through SnO_2 in our SnO_2–In_2O_3 composites occurs at a total SnO_2 concentration of about 40 wt %.

Sensor effect S in the studied SnO_2–In_2O_3 nanocomposites, as well as in other nanostructured metal oxide sensors, varies with temperature and, at a certain temperature value T_{max}, it achieves a maximum value S_{max} (Fig. 3). The dependence of S_{max} on the SnO_2 concentration in the case of hydrogen detection by an

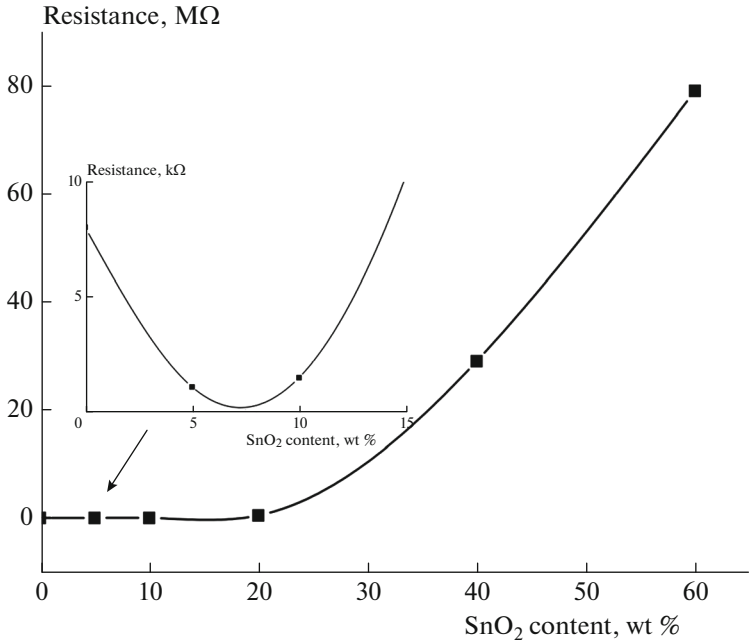

Fig. 1. Dependence of the resistance of the impregnated SnO_2–In_2O_3 composite on the SnO_2 content.

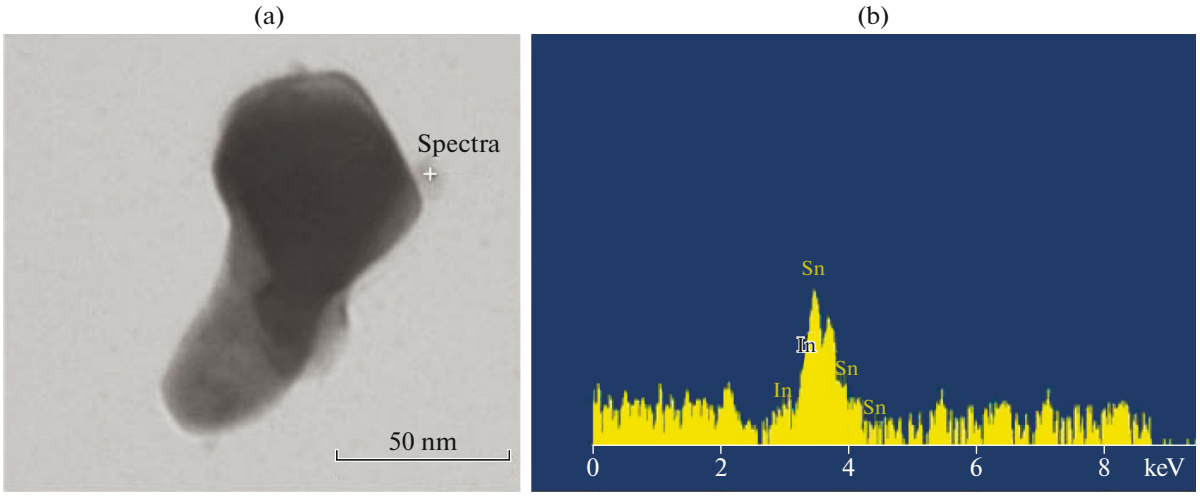

Fig. 2. (a) Transmission electron microscopy image of an In_2O_3 composite particle with a SnO_2 cluster on the surface and (b) EDX spectra of a SnO_2 cluster.

impregnated SnO_2–In_2O_3 composite sensor is shown in Fig. 4. Small SnO_2 additives (up to 10 wt %), which dissolve in In_2O_3 crystals, lead simultaneously to an increase in the conductivity and a decrease in the sensor effect. Earlier, a decrease in S with an increase in the conductivity of the nanocrystalline sensor was found for SnO_2 sensor films synthesized by the aerosol method [20].

At low SnO_2 concentrations in SnO_2–In_2O_3 composites, current flows through the In_2O_3 crystals. In this case, one possible cause of a decrease in the sensor effect is an increase in the conduction electron concentration n_c upon the introduction of Sn ions into the In_2O_3 lattice. The S value is defined as the ratio of the rate of the reaction of the analyte reducing gas with oxygen anions O^- (V_r) to the rate of the annihilation of these anions in the absence of the gas (V_O) [1, 2]. The V_r/V_O ratio is determined by the annihilation mechanism of O^- in the absence of the gas.

In the case of monomolecular annihilation due to the electron detachment from the O^- anion [1, 9], the $V_r/V_O = k_r[A]/k_{O1}$ ratio does not depend on $[O^-]$; here, k_r is the rate constant for the reaction between O^- and the adsorbed gas, [A] is the adsorbed gas concentration, and k_{O1} is the $O^- \rightarrow O + e^-$ reaction rate constant. In the case of annihilation of O^- due to the

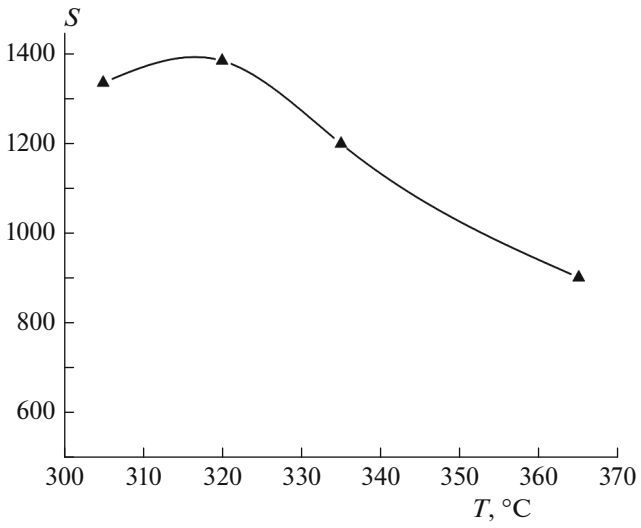

Fig. 3. Temperature dependence of the sensor response S of a 40% SnO_2–60% In_2O_3 nanocomposite film synthesized by the impregnation method.

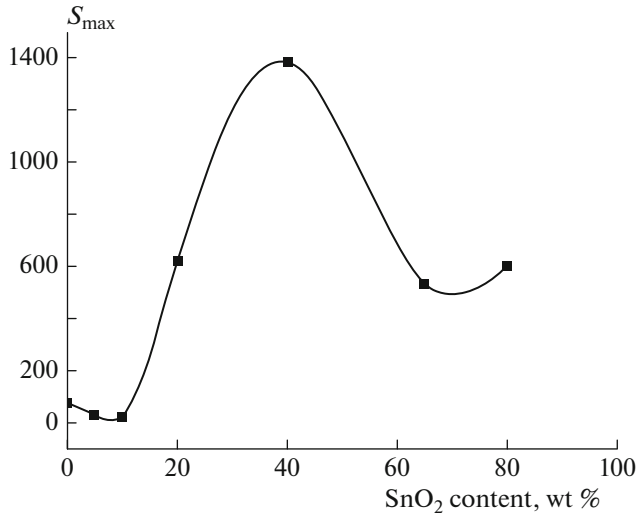

Fig. 4. Dependence of the maximum sensor effect S_{max} in SnO_2–In_2O_3 composites on the SnO_2 content.

bimolecular reaction $2O^- \rightarrow O_2 + 2e^-$ with rate constant k_{O2} [2], the V_r/V_O ratio is determined by the following equation: $V_r/V_O = k_r[A]/k_{O2}[O^-]$. An increase in n_c unambiguously leads to an increase in $[O^-]$; therefore, in this case, the V_r/V_O ratio and, accordingly, the S value should decrease with increasing n_c. Apparently, in the studied system, the annihilation of O^- on the In_2O_3 surface occurs via the recombination of these radical anions; this factor is responsible for the decrease in S with an increase in n_c, owing to the incorporation of Sn ions into the In_2O_3 lattice.

The percolation transition to conduction through SnO_2, which is accompanied by an increase in the resistance of the composite, leads to a gradual increase in the sensor effect (Fig. 4). It is characteristic that the maximum value of the sensor effect is achieved at 40 wt % SnO_2, when, in accordance with the percolation theory, the final percolation transition to conduction through SnO_2 nanoclusters occurs in the composite.

Aggregates of SnO_2 nanoclusters contacting each other, which form current paths in this composite, have an exceptionally high specific surface area. This factor is a cause of the enhancement of the sensor effect after the percolation transition to conduction in the composite through SnO_2 because, according to theoretical analysis [9, 21] and experimental data [22], the sensor effect in a nanostructured system increases with an increase in the specific surface area of this system. Another cause is the structure of SnO_2 particles contacting with In_2O_3 crystals. The EDX data (Fig. 2b) show that these particles contain In ions, due to the dissolution of In_2O_3 in SnO_2.

The formation of a solid solution of In_2O_3 in SnO_2 is facilitated for SnO_2 nanoparticles, because they are more readily deformed upon the replacement of Sn^{4+} ions by the larger In^{3+} ions in the SnO_2 lattice, so that, in small SnO_2 particles, the fraction of dissolved In with respect to Sn in the nanoclusters can be up to 20% [11]. The dissolution of In_2O_3 in SnO_2 can be represented by the following equation [23]:

$$In_2O_3 + 2Sn_{Sn} + O_O \leftrightarrow 2In'_{Sn} + V_O^{++} + 2SnO_2,$$

where Sn_{Sn} and O_O are the Sn^{4+} and O^{2-} ions in the SnO_2 lattice, In'_{Sn} is the In^{3+} ion that replaces Sn^{4+} in the SnO_2 lattice and generates a localized negative charge in the lattice, and V_O^{++} is the positively charged oxygen vacancy compensating for the negative charge at In'_{Sn}. The formation of positively charged oxygen vacancies leads to a decrease in n_c and, accordingly, the conductivity of the composite. In addition, these vacancies are centers of hydrogen adsorption to form H atoms [24]; therefore, they increase the catalytic activity of the composite in the sensory reaction of analyte hydrogen with O^- radical anions on the surface of SnO_2 nanoparticles.

It is characteristic that the sensor effect increases with an increase in the SnO_2 concentration to 40 wt % and then decreases (Fig. 4). This result can be attributed to the fact that, in the In_2O_3–SnO_2 composites, at a SnO_2 content of 40 wt %, the concentration of SnO_2 nanoclusters contacting with In_2O_3 crystals and containing indium ions, which increase the catalytic activity of these nanoparticles in the sensory reaction, apparently achieves a maximum.

Thus, the high sensor sensitivity of the composite is attributed to the following: the catalytic activity of SnO_2 particles containing indium ions in the dissociative chemisorption of H_2 and the small (5–7 nm) size of these particles, which, in accordance with the percolation theory, determine the conductivity of the composite at a SnO_2 content of more than 30 wt %. In this case, the aggregates of SnO_2 particles that form the current paths have a particularly high specific surface area, which increases the sensor response of the composite. Another factor that causes an increase in the sensor response of the composite under these conditions may be electron transfer from In_2O_3 to SnO_2, which increases due to the sensor reaction. This conclusion follows from the results of studies of In_2O_3–SnO_2 composites synthesized by mixing In_2O_3 and SnO_2 nanopowders [7]. It is obvious that the degree of electron transfer between In_2O_3 and SnO_2 is maximal if the concentration of SnO_2 nanoparticles contacting with In_2O_3 crystals achieves a maximum value.

CONCLUSIONS

The structure and sensing properties of a SnO_2–In_2O_3 composite synthesized by the impregnation of In_2O_3 nanocrystals with an aqueous solution of $SnCl_4$ and the subsequent formation of SnO_2 nanoclusters during the heat treatment of the impregnated samples have been studied. It has been shown that this method provides the formation of SnO_2 nanoclusters with a size of 5–7 nm on the surface of In_2O_3 crystals. Using EDX spectroscopy, it has been found that these SnO_2 nanoclusters contain indium ions; therefore, the number of catalytically active oxygen vacancies in the clusters increases.

The maximum efficiency of hydrogen detection in air by the synthesized SnO_2–In_2O_3 composite sensors is achieved at a SnO_2 content in the composite of about 40 wt %, when, according to the percolation theory, the current paths are aggregates of SnO_2 clusters contacting with In_2O_3 crystals. In this case, the high sensor sensitivity of the composite is attributed to the catalytic activity of SnO_2 clusters containing indium ions and the high specific surface area of SnO_2 aggregates providing the conductivity of the composite.

FUNDING

This work was performed under a state task to Semenov Institute of Chemical Physics of the Russian Academy of Sciences (project 45.22 no. 0082-2018-0003 "Fundamentals of Designing New-Generation Nanostructured Systems with Unique Performance Characteristics" (AAAA-A18-118012390045-2)) and supported by the Russian Foundation for Basic Research (project nos. 17-07-00131a, 18-07-00551a, 19-07-00141a, and 19-07-00251a).

REFERENCES

1. N. Barsan and U. Weimar, J. Electroceram. **7**, 143 (2001).
2. N. Yamazoe and K. Shimanoe, Sens. Actuators, B **128**, 566 (2008).
3. G. N. Gerasimov, V. F. Gromov, O. J. Ilegbusi, and L. I. Trakhtenberg, Sens. Actuators, B **240**, 613 (2017).
4. V. Brinzari, I. Damaskin, L. Trakhtenberg, et al., Thin Solid Films **552**, 225 (2014).
5. L. I. Trakhtenberg, G. N. Gerasimov, L. N. Aleksandrova, and V. K. Potapov, Radiat. Phys. Chem. **65**, 479 (2002).
6. W. J. Moon, J. H. Yu, and C. G. Man, Sens. Actuators, B **87**, 464 (2002).
7. L. I. Trakhtenberg, G. N. Gerasimov, V. F. Gromov, et al., Sens. Actuators, B **169**, 32 (2012).
8. K.-W. Kim, P.-S. Cho, S.-J. Kim, et al., Sens. Actuators, B **123**, 318 (2007).
9. M. A. Kozhushner, L. I. Trakhtenberg, V. L. Bodneva, et al., J. Phys. Chem. C **118**, 11440 (2014).
10. G. Korotcenkov, S.-D. Han, B. K. Cho, and V. Brinzari, Crit. Rev. Solid State Mater. Sci. **34**, 1 (2009).
11. K. I. Gnanasekar, X. Jiang, J. C. Jiang, et al., J. Nanosci. Nanotechnol. **2**, 189 (2002).
12. M. M. Natile and A. Glisenti, J. Phys. Chem. B **110**, 2515 (2006).
13. G. N. Gerasimov, M. I. Ikim, P. S. Timashev, V. F. Gromov, T. V. Belysheva, E. Yu. Spiridonova, V. N. Bagratashvili, and L. I. Trakhtenberg, Russ. J. Phys. Chem. A **89**, 1059 (2015).
14. V. F. Gromov, G. N. Gerasimov, T. V. Belysheva, M. I. Ikim, E. Yu. Spiridonova, M. M. Grekhov, R. A. Ali-zade, and L. I. Trakhtenberg, Russ. J. Phys. Chem. B **12**, 129 (2018).
15. G. N. Gerasimov, M. M. Grekhov, V. F. Gromov, M. I. Ikim, E. Yu. Spiridonova, and L. I. Trakhtenberg, Russ. J. Phys. Chem. B **12**, 709 (2018).
16. H. Kim, C. M. Gilmore, A. Piqué, et al., J. Appl. Phys. **86**, 6451 (1999).
17. S. J. Wen, G. Coutirier, J. P. Chaminade, et al., J. Solid State Chem. **101**, 203 (1992).
18. H. Enoki, J. Echigoya, and H. Suto, J. Mater. Sci. **26**, 4110 (1991).
19. N. Savage, B. Chwieroth, A. Ginwalla, et al., Sens. Actuators, B **79**, 17 (2001).
20. G. Korotcenkov, V. Brinzari, J. Schwank, et al., Sens. Actuators, B **77**, 244 (2001).
21. M. A. Kozhushner, L. I. Trakhtenberg, A. C. Landerville, et al., J. Phys. Chem. C **117**, 11562 (2013).
22. G. J. Li, X. H. Zhang, and S. Kawi, Sens. Actuators, B **60**, 64 (1999).
23. J. Maier and W. Gopel, J. Solid State Chem. **72**, 293 (1988).
24. W. Gopel, G. Rocker, and R. Feierabend, Phys. Rev. B **28**, 3427 (1983).

Translated by M. Timoshinina